

A Review on Antimony-based Perovskite Solar Cells

Ankit Stephen Thomas^{a,*}

Department of Chemical Engineering, National Institute of Technology Karnataka, India

*Corresponding author: ankitstomas@gmail.com

DOI: <https://dx.doi.org/10.20961/equilibrium.v6i2.64322>

Article History

Received: 06-08-2022, Accepted: 14-10-2022, Published: 15-10-2022

Keywords:
Perovskite Solar
Cells, Photovoltaic
Technology, Lead-
free Perovskites,
Solar Cell
Materials,
Antimony-based
Perovskites

ABSTRACT. Over the past decade, lead halide perovskite light absorbers have been the conventionally used perovskite light absorbers. However, there is an urgent call for alternative perovskite materials with toxicity levels and poor stability to UV radiations. Antimony-based perovskites have proven to be a material with unique optoelectronic properties, conventional fabrication processes, low-toxicity levels and high stability values. In this review, we look into the structure of antimony perovskites, the various research achievements over recent years, and the challenges and opportunities ahead for this budding technology. The review also highlights the various computational, theoretical and experimental studies done by researchers to highlight the peculiar Lead-free perovskite materials and their distinctive features. Although the efficiency levels of these devices are not very high, the improvements they have made with remarkable stability characteristics make them a viable candidate for commercial perovskite photovoltaics.

1. INTRODUCTION

Solar cell technologies are primarily divided into three generations, namely the first, second and third generation. The first generation of photovoltaic technologies include the conventional monocrystalline and polycrystalline solar cells. The issue with this generation of devices is, it is very expensive, the processing conditions and fabricating procedures of these devices are very difficult. Moreover, once the solar cell has completed its lifetime, issues regarding waste disposal and management arise. The second generation of solar cells are thin film photovoltaics such as GaAs, CdTe and CIGS. The issue with this domain is the rarity in finding the materials, expensive usage applications and toxic materials like cadmium (Cd) being used. Lastly, third generation photovoltaics is a family of solar cells including thin-film, multi-layer and tandem devices. The advantages of third generation solar cells are the low-cost materials used, seamless fabrication procedures and high photon to electron conversion efficiencies. Amongst the third generation of photovoltaics, the most emerging technology is perovskite solar cells [1].

The table 1 shows a list of the various available solar cell technologies along with their maximum theoretical efficiencies achieved [2].

Table 1. Comparison of photovoltaic technologies and efficiencies

Solar cell device type	Maximum efficiency observed (%)	Ref.
Single-crystalline Si	27.6	[2]
Multi-crystalline Si	24.3	[2]
Thick Si film	24.7	[2]
CdTe	12.1	[2]
CIGS	19.9	[2]
Perovskite	25.7	[2]
Dye-sensitized	11.1	[2]
Organic	9.4	[2]

Perovskite Solar Cells (PSCs) have attracted significant attention for their unique optoelectronic properties, tuneable energy bandgap, easy fabrication process, abundant material sourcing, and cheap and efficient results.

The typical active material used in a PSC is typically $\text{CH}_3\text{NH}_3\text{PbI}_3$ (MAPbI_3 – Methylammonium Lead Iodide) [1].

It is important to note that a perovskite molecule follows the general molecular formula of ABX_3 , where A is a large cation, typically MA^+ and FA^+ . B is a smaller cation usually belonging to the transition group elements (Pb), and X is a halide anion (Cl, Br, F⁻). Lead-based perovskites have shown tremendous success over the previous years. The reasons for this are high absorption coefficient, suitable bandgap, reduced defects, low-temperature processability, solution-processable and long carrier lifetimes. However, lead-based perovskites cannot be commercialised for the following reasons: low stability properties towards UV radiation, heat and moisture, and high toxicity levels. This calls for more efficient, sustainable and eco-friendly alternatives [3].

Reports have also conducted tests, like life cycle assessments (LCA), to measure the ecological balance, environmental impact and cost-benefit analysis of perovskite solar technologies. This investigates the device fabrication, from sourcing the materials to deposition and fabricating the entire device. The results from LCA studies indicate significant contamination occurring due to Pb-based perovskites, especially in the processing stage. Moreover, other reports have suggested that fabricating devices using Pb-based perovskites has resulted in air and water contamination, damage of local ecosystems and degradation of workers' health. Therefore, this gives us more reasons to shift towards greener, safer and highly-efficient perovskite devices [4].

Various other alternatives to replace Pb have been like Bi, Sb, Ge and Sn. It is important to note that, before replacing the Pb in a perovskite material, we need to study the impact of the alternatives on the environment. Sn^{2+} and Ge^{2+} get oxidised easily to Sn^{4+} and Ge^{4+} , respectively, which makes it extremely difficult to work with in a PSC. Moreover, Sn-based perovskites are toxic as well. Hence the only viable alternatives are Bi and Sb-based perovskites, which belong to the same group (VA) in the periodic table. Unlike Sn and Ge, Bi and Sb are trivalent cations (Bi^{3+} and Sb^{3+}) with an ionic radius similar to Pb^{2+} . From this section, we can conclude that researchers and policy makers need to develop and develop a structured framework that investigates alternatives for Pb on a thorough basis, from processing costs to material sourcing availability [5].

Sb-based halide perovskites have been developed in the past and are currently being used on a very temporary scale. They have been identified as suitable alternatives to behave as light absorbers. $\text{MA}_3\text{Sb}_2\text{I}_9$ and $\text{Cs}_3\text{Sb}_2\text{I}_9$ are a few of the typical Sb-based light absorbers developed. However, these materials have extremely wide bandgaps, high binding energies and high carrier effective masses, which further limits the photovoltaic performance [3]. This is why VA-based halide perovskites are not being implemented extensively, with performances much lower than Pb-based perovskites.

The previous theoretical and experimental studies on Sb-based PSCs are only limited to its performance and future prospects in terms of scalability. In this review, we shall look into how Antimony perovskites are synthesised, the molecular structure of Sb-based perovskites. The computational and theoretical studies on Sb-based perovskite materials are also covered in this article, and how theoretical and experimental results can be correlated, especially on an optoelectronic basis. The general molecular structure ($\text{A}_3\text{Sb}_2\text{X}_9$) is elaborated upon, along with the recent progress, challenges, barriers to commercialisation and further opportunities for research. Lastly, the stability properties and strategies to improve device stability and performance is elucidated in detail.

2. FABRICATION OF ANTIMONY-BASED PEROVSKITES

Perovskite films are generally produced through solution-processable methods. However, they can also be prepared through vapour-assisted methods. The photovoltaic performance depends strongly on the film quality, which indirectly depends on the synthesis method. When a solution-processable method is typically used, factors like the age of chemicals, solvent boiling point, atmospheric conditions and coordinating strength impact the film quality and its optoelectronic properties [6].

The one-step deposition method is the most commonly used. In this case, halides of A and B cation salts are dissolved in a polar solvent and then spin-coated onto a substrate. Perovskite films with larger grain sizes are preferred as they reduce grain boundaries and improve charge transport across the material. The perovskite precursor solutions have solvated ions and colloidal networks that directly impact the crystal growth of the perovskite crystal. The interaction between the metal halides and the solvent molecules plays a vital role in determining film morphology. If the species are firmly coordinated, perovskite nucleation and crystal growth tend to slow down.

Moreover, the solvent used in one-step deposition plays an essential role in perovskite film morphology. There is a technique that is known as antisolvent washing that is used after the perovskite crystals are formed. This is

done to remove the perovskite precursor solvents. The choice of antisolvent used also plays a significant role in determining the morphology and quality of the film [7].

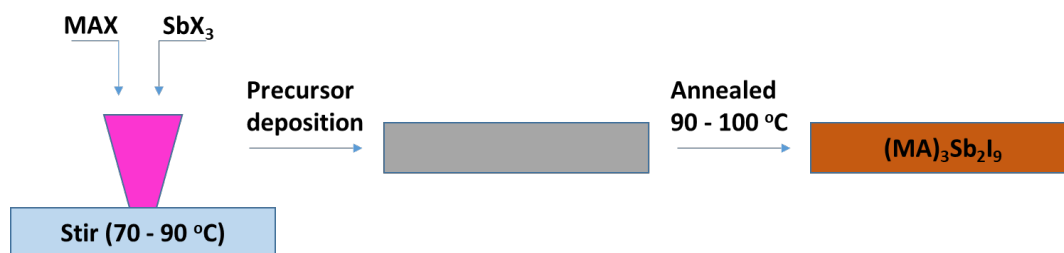


Figure 1. Schematic representation of Sb-film synthesis

A two-step deposition method includes, firstly, deposition of metal halide, followed by interdiffusion of organic salt. Through this method, the film produced is not just homogeneous. It is uniform, has better wettability and has reduced notable defects. The organic salt must penetrate the inorganic salt.

This ensures that the perovskite film obtained has a suitable thickness. The deposition of the first layer can be further improved by using additives and restructuring the metal halides [6]. Figure 1 clearly represents the processes required to synthesise a Pb-free perovskite film.

3. STRUCTURE OF ANTIMONY-BASED PEROVSKITES

As mentioned earlier, Sb, a trivalent cation, has three electrons in its valence shell. Thus, when a trivalent cation replaces Pb^{2+} , the resulting ionic compound formed will be of the form SbX_6^{3-} . This is an octahedron-shaped molecule where halide ions are coordinated to the A cation to give rise to a perovskite molecule with different dimensionality and structure. The molecular formula of $\text{A}_3\text{B}_2\text{X}_9$ usually produces perovskite molecules that are 0-dimensional (0D) or 2-dimensional (2D) [3]. However, the case of double perovskites with a molecular formula of $\text{A}_2\text{B}^{\text{I}}\text{B}^{\text{III}}\text{X}_6$ has a 3-dimensional (3D) structure where the B^{I} and B^{III} cations are corner-sharing molecules.

When incorporated into a PSC, Sb-based perovskites possess highly unique and exceptional optoelectronic properties. These materials have been tested computationally and experimentally to study the optical properties of 0D and 2D forms.

0D is a dimeric form, and 2D is a layered form of the $\text{Cs}_3\text{Sb}_2\text{I}_9$. CsSbI_3 can be produced in a hypothetical scenario by structurally modifying the $\text{Cs}_3\text{Sb}_2\text{I}_9$ layers [8]. 2D $\text{Cs}_3\text{Sb}_2\text{I}_9$ has an optical bandgap of 2.05 eV and is regarded for its enhanced stability in ambient conditions compared to MAPbI_3 . The Cs atom can be replaced with other alkali atoms like Rb or K. It is important to note here that the A cation plays a critical role in the optoelectronic properties of the material. It can impact the bandgap by tuning it to a direct or indirect bandgap. Rb and K-based Sb halide perovskites have a direct bandgap and a 2D structure due to their smaller ionic radius stabilising the 2D structure [9]. Colloidal $\text{Cs}_3\text{Sb}_2\text{I}_9$ and $\text{Rb}_3\text{Sb}_2\text{I}_9$ nanocrystals have been synthesised previously, with high absorption coefficients and a 2D structure [10]. Thus, making them suitable candidates as perovskite light absorbers.

A Cu-doped Sb-based halide perovskite was recently synthesised with an indirect bandgap of 1.02 eV. This was compared to $\text{Cs}_2\text{SbAgCl}_6$ with a bandgap of 2.65 eV [11]. Double-layered perovskites with the molecular formula of $\text{Cs}_{3+n}\text{M}(\text{II})_n\text{Sb}_2\text{X}_{9+3n}$ with octahedral layers of $[\text{GeI}_6]$ and $[\text{SnI}_6]$. This modification enhanced structural stability, increased electronic dimensionality, reduced bandgap and binding energies, and higher absorption properties [12]. Vargas and coworkers developed an Mn and Cu, Sb-based halide perovskite. Through this study, it was shown that on varying the Mn and Cu ratios, the bandgap of the perovskite molecule could be adjusted. In addition to this, physical characteristics like magnetoelectric properties can be tuned using molecular, sidechain or compositional engineering [13].

Jakubas and Bagautdinov's works suggested that they synthesised $\text{MA}_3\text{Sb}_2\text{I}_9$ and $\text{Cs}_3\text{Sb}_2\text{I}_9$, respectively and studied their related properties [14,15]. Yang and coworkers showed and concluded that by replacing I⁻ with Br⁻, the resulting perovskite possesses a trigonal crystal structure [16]. Zhang and coworkers synthesised $(\text{NH}_4)_3\text{Sb}_2\text{I}_9$ and showed that it crystallises in a monoclinic crystal form [17]. Zuo and coworkers synthesised $(\text{NH}_4)_3\text{Sb}_2\text{I}_9$ through an antisolvent vapour-assisted crystallisation method. The resultant perovskite molecule formed an octahedron with Nitrogen atoms at the centre, forming a tetrahedron [18].

Buonassisi and coworkers studied the optoelectronic and photovoltaic properties of $\text{Cs}_3\text{Sb}_2\text{I}_9$, $\text{K}_3\text{Sb}_2\text{I}_9$ and

Rb₃Sb₂I₉ perovskite materials. It was found that the materials possessed a 0D, 2D and 2D crystal structure, respectively [9].

Table 2 explains the film characteristics of various Sb-based perovskites, their film and crystal properties and variation with charge carrier type.

Table 2. Charge carrier mobility of Antimony perovskites

Material	Film type	Charge carrier type	Charge carrier mobility (cm ⁻¹ V ⁻¹ s ⁻¹)	Ref.
(MA) ₃ Sb ₂ I _x Br _{9-x}	Single crystal	Electron	12.3	[19]
(MA) ₃ Sb ₂ I _x Br _{9-x}	Single crystal	Hole	4.8	[19]
(MA) ₃ Sb ₂ I ₉	Single crystal	Hole	4.8	[19]
(MA) ₃ Sb ₂ I ₉	Single crystal	Electron	12.3	[19]
(MA) ₃ Sb ₂ I ₉	Film	Hole	1.2 x 10 ⁻⁴	[19]
(MA) ₃ Sb ₂ I ₉	Film	Electron	1.5 x 10 ⁻⁴	[19]

4. COMPUTATIONAL STUDIES ON ANTIMONY-BASED PEROVSKITES

Sb-based double perovskites have been studied theoretically and computationally using specific analyses like DFT/LDA. The results showed that most of the double perovskites possessed an indirect bandgap. However, suitable modifications and experimental strategies could convert these to a direct bandgap [20].

A total of eleven double perovskites were developed and screened based on thermodynamic stability, optoelectronic stability and bandgap values. Cs₂InSbCl₆ was one of the two materials that displayed a direct bandgap of 1.0 eV [21]. Deng and coworkers produced a double perovskite Cs₂AgSbCl₆. As per computational results, the material showed an indirect bandgap of 2.41 eV. The experimental results show a similar value of 2.60 eV.

Coupling Cs₂AgSbCl₆ with TiO₂ heterostructures showed improved light absorption properties. Sb₂S₃, Cs₂Sb₈S₁₃ and MA₂Sb₈Sb₁₃ are a few of the other compounds that have been investigated for their unique structure and electronic properties [21]. Through computational results, the observed bandgap values were 1.72, 1.85 and 2.08 eV, respectively. Deng and coworkers also synthesised an Antimony-Silver double perovskite of the formula (CH₃NH₃)₂AgSbI₆ with a bandgap of 1.93 eV and enhanced stability of 370 days [22].

Computational results have also shown that a mixed-metal-halide perovskite: (CH₃NH₃)₂AgSbI₆ possessed a bandgap of 2.0 eV. This value was verified through experimental results by synthesising MA₂AgSbI₆ with a bandgap of 1.93 eV [22].

VA-based halide perovskites (Bi and Sb) have been suggested as alternatives to Pb-halide perovskites. The reasons for this transition are a) low toxicity, b) high structural stability, and c) more excellent UV, moisture and temperature stability. With these advantages and the rate at which these materials are progressing in recent times, improved PCE and commercialisation will be possible in the long run. Figure 2 depicts a typical device employing an Sb-based perovskite layer as the light absorber and the corresponding energy level diagram for all the device components.

Zuo and coworkers showed that (NH₄)₃Sb₂I₉ has an optical bandgap of 2.27 eV [23]. In contrast, Boopathi and coworkers showed that Cs₃Sb₂I₉ has a bandgap of 1.95 eV and MA₃Sb₂I₉ has a bandgap of 2.0 eV [24]. Buonassisi and coworkers found that the optical bandgap of Cs, Rb and K-based Sb-Iodide perovskites are 2.43, 2.03 and 2.02 eV, respectively, through UV-Vis absorption spectroscopy.

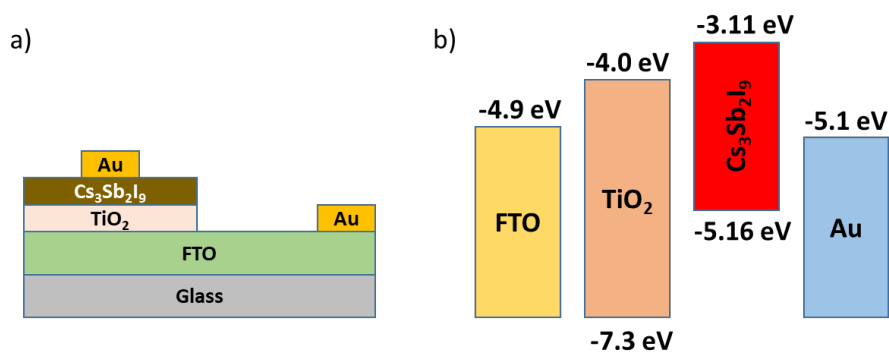


Figure 2. a) Schematic diagram of Cs-Sb PSC, b) Energy level diagram of device materials

5. ANTIMONY HALIDE PEROVSKITES

5.1 Cs₃Sb₂I₉ Perovskites

As mentioned earlier, Sb can form several various organic and inorganic cations. Cs₃Sb₂I₉ forms different solid structures. The solution processed form is a 0D structure, whereas the 2D-layered structure is formed through solid or gas reactions. In 2015 when Cs₃Sb₂I₉ was first used as a light absorber. Saparov and coworkers determined that the 2D structure has a bandgap of 2.05 eV, an absorption coefficient of 10⁵ cm⁻¹ and an ionisation potential of 5.6 eV. The stability reported is much higher than MAPbI₃, especially in ambient atmospheres. The PCE produced using Cs₃Sb₂I₉ as a light absorber was less than 1%. This is because of its high recombination probability and defect states [25].

Similarly, the 0D structure (bandgap of 2.0 eV) was also used in PSCs. Correa-Baena and coworkers showed that the low photocurrent values are attributed to its indirect bandgap and high binding energy [26]. Chu and coworkers developed a planar PSC device to obtain a PCE of 0.67% [27]. On using HI as an additive, the device produced a PCE of 0.84%. A V_{oc} of 0.60 V. Furthermore, a layered and dimeric variant of Cs₃Sb₂I₉ was prepared through a vapour-assisted solution processable method. For the layered variant, the lifetime and binding energy values were 6 ns and 100 meV, respectively. Including the layered and dimeric form into a PSC yielded a PCE of 1.5% and 0.89%, respectively. Zhou and coworkers synthesised a MA₃Sb₂Cl_xI_{9-x} by adding Methylammonium Chloride into the precursor solution [28].

Zhubing He and his coworkers attempted to solve this issue using Hydrochloric Acid (HCl) as an additive [30]. Using this method, Chlorine acted as an inhibitor to resist the formation of Sb-I-Sb bonds. This eventually produced a layered Cs₃Sb₂I₉ film with a bandgap of 2.05 eV. It is important to note that the observed bandgap value is lower than its dimeric form (2.47 eV). Incorporating the layered structure into a PSC produced a PCE of 1.21%, whereas the dimeric form produced only 0.43%. This variation in PCE level can be attributed to the reduced trap states, improved carrier mobility and junction quality. The addition of HCl essentially resolved the dimeric form nature of Cs₃Sb₂I₉.

Umar and coworkers fabricated mesoporous PSCs using Cs₃Sb₂I₉ [29]. The Cs₃Sb₂I₉ films formed are of exceptionally high film quality and tend to exist in the dimeric form. In this study, a dimer phase was produced, and a layered phase was produced using HCl. The films were synthesised with and without antisolvents. The results showed that antisolvents yielded films with reduced pinholes and trap states, especially isopropanol. The highest PCE obtained was 1.21% from a device using HCl. Singh and coworkers produced a modified Cs₃Sb₂I₉ phase (layered polymorph phase) [27]. On incorporating this material into a PSC, the photovoltaic performance was 1.5% higher than its dimer counterpart. The improved photovoltaic performance can be related to the lower bandgap values and unique optoelectronic properties of the layered structure.

Moreover, Chonamada and coworkers also studied the stability characteristics of layered and dimer forms of Cs₃Sb₂I₉ profoundly [30]. Figure 5 shows an accurate flowchart-based representation of how the layered and dimeric forms of Cs₃Sb₂I₉ perovskite materials can be synthesised. The stability was studied under humidity, light and heat. The humidity studies observed that both the films hydrated and decomposed into CsI, Sb₂O₃ and HI. When HI was added, the reaction was seen to be reversed. The thermal studies noted that both the films decomposed to SbI₂ and CsI, which can be recovered quickly. However, the vital point to note here is that the layered variant showed excellent stability against heat. Under the light studies, both films began to decompose through photoinduced degradation. Once these samples were stored in a dark environment, no notable degradation

was noted. It was observed that the dimer form of the material degraded after 49 days. In contrast, the layered form degraded only after 88 days. These results further validate why $\text{Cs}_3\text{Sb}_2\text{I}_9$ is a viable candidate as a light absorber for photovoltaic applications.

5.2 $\text{Rb}_3\text{Sb}_2\text{I}_9$ Perovskites

Harikesh and coworkers developed a solution-processable method of the same Sb-based perovskite. However, the Cs atom was replaced by Rb [31]. Moreover, due to the smaller ionic radius of Rb, the resulting perovskite will be of a layered structure. Similar to its Cs-counterpart, the Rb-Sb-based perovskite displayed enhanced thermal stability, which is a valuable property in a PSC. However, its sizeable indirect bandgap (2.1 eV) makes it unfavourable for optimal photovoltaic performance. Coupling this material with poly-TPD as the HTM resulted in a PCE of 0.66%.

From the above work, one can conclude that the A cation plays more than just a significant role in determining photovoltaic performance. A cation can directly or indirectly impact produced films' structural and optoelectronic properties. Moreover, it also influences the exciton binding energy, carrier charge effective masses and produced photocurrents. The most significant efficiency obtained by using an Rb-based Sb perovskite is 0.76% [9]. Weber and coworkers showed that the crystal structure is not affected by replacing the Iodide ion with Bromide [32]. However, there is a notable increase in the bandgap and the PCE obtained is nearly 1.3%. Additionally, there is a notable improvement in device stability for up to 150 days, and 85% of its initial PCE is retained.

$\text{Rb}_3\text{Sb}_2\text{I}_9$ is a potential candidate for PSCs due to its favourable absorption coefficient and improved stability. Incorporating Rb as an A-site cation improves the material's structural, dimensional and optical properties and influences the binding energy and, eventually, the photovoltaic performance of the material. Buonassisi and coworkers fabricated PSCs using K, Rb and Cs-based Sb-halide perovskites [26]. The results showed that the Rb-based device exhibited improved efficiency, and the K and Cs-based device showed lower efficiency values.

A perovskite film with a large grain size directly impacts the device's performance to improve carrier mobility and lifetime. Therefore, the photovoltaic performance using various materials can be directly improved by tuning charge mobility values, diffusion lengths and carrier drift. Li and coworkers synthesised $\text{Rb}_3\text{Sb}_2\text{I}_9$ using various methods and studied the dependency of photovoltaic performance on synthesis methods [33]. It was observed that the highest device performance was obtained from the high-temperature vapour annealing method (HTVA) with a grain size of 600 nm. The increase in device efficiency can be associated with larger grains, greater carrier mobility and lifetime values.

5.3 $\text{MA}_3\text{Sb}_2\text{I}_9$ Perovskites

Hebig and coworkers synthesised solution processable $\text{MA}_3\text{Sb}_2\text{I}_9$, which possesses a hexagonal shape [34,35]. Moreover, amorphous $\text{MA}_3\text{Sb}_2\text{I}_9$ shows an absorption coefficient of 10^5 cm^{-1} , an optical bandgap of 2.14 eV and significant energy disorder. All the synthesised Sb-based pure halide perovskites have bandgaps greater than 2 eV. The $\text{MA}_3\text{Sb}_2\text{I}_9$ film produced through a one-step method produced a crystalline film. In comparison, the film produced through a two-step method was amorphous. This amorphous nature can be attributed to the presence of Toluene. Moreover, the hexagonal structure of $\text{MA}_3\text{Sb}_2\text{I}_9$ was visible in the one-step method, but a pinhole-free and non-hexagonal structure was obtained in the two-step method [36].

Studies have shown that $\text{MA}_3\text{Sb}_2\text{I}_9$ incorporation into a planar PSC produced a PCE of 0.49% and a V_{oc} of 896 mV. The device components used in this case were: ITO/PEDOT:PSS/ $\text{MA}_3\text{Sb}_2\text{I}_9$ /PC61BM/ZnO-NP/Al [37]. Giesbrecht and coworkers synthesised the 2D form of $\text{MA}_3\text{Sb}_2\text{I}_9$ in a glovebox using Antimony Acetate [38]. The results showed that the 2D version produced improved results than its 0D counterpart. The PSCs were fabricated using mesoporous TiO_2 and compact SnO_2 (c- SnO_2). It was observed that the mesoporous-based device yielded higher efficiency values (0.54%) than the c- SnO_2 device (0.36%). However, the higher V_{oc} value was reported for the c- SnO_2 -based device due to its lower recombination rates and high film quality.

Shaikh and coworkers synthesised $\text{MA}_3\text{Sb}_2\text{I}_9$ using a two-step sequential deposition method with an indirect bandgap of 2.1 eV [35]. On fabricating a PSC device with this material, a moderate PCE of 0.54% was obtained with a V_{oc} of 740 mV. These values were higher than the devices produced through a one-step deposition method. The higher photovoltaic performance is attributed to the improved film quality, surface morphology, homogeneity, charge extraction and transportation.

Boopathi and coworkers showed that by using Hydroiodic Acid (HI) as an additive with varying precursor concentrations, the optimal device efficiency is found to be 2.04% and 1.11% for a device without HI additive

[38].

Studies have been conducted where PSCs were fabricated using Cu@NiO as a hole transporting material and ZnO as the electron transporting material [39]. The active layer used in this case was $\text{MA}_3(\text{Sb}_{1-x}\text{Sn}_x)_2\text{I}$, and the highest efficiency obtained was 2.69%. This research showed that $\text{MA}_3\text{Sb}_2\text{I}_9$ has favourable bandgap and morphological features, which make that suitable for PSCs. Figure 3 displays the device architecture of one of the highest performing Sb-based devices, where the addition of Pyrene, HI and Chlorobenzene are pointed out clearly.

As discussed, MA^+ , as the A site cation, produces only the dimeric 0D form. However, the material's many energy disorders and high binding energy result in reduced photocurrent and PCE values lower than 0.5%.

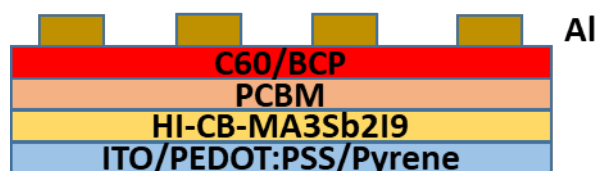


Figure 3. Sb PSC with a hydrophobic layer, HI and Chlorobenzene as additives

The morphology of the film plays a vital role in device performance. Karuppuswamy and coworkers synthesised large grain crystals of $\text{MA}_3\text{Sb}_2\text{I}_9$ [38]. They employed a growth regulation technique wherein HI was used as the additive, chlorobenzene antisolvent treatment and a hydrophobic HTM. The fabricated device showed fewer voids and improved film quality. The resultant efficiency was 2.77%, with reduced interfacial resistance than the standard PEDOT:PSS device. Dai and coworkers showed how $\text{MA}_3\text{Sb}_2\text{I}_{9-x}\text{Cl}_x$ 2D films could be produced using a Lithium bi(trifluoromethane)sulfonamide (Li-TFSI). The resultant efficiency was more significant than 3%, the highest PCE recorded for a pure Sb-based PSC [39]. The resulting material has a bandgap of 2.05 eV, yields a PCE of 3.34 % and enhanced stability of more than 1400 hours in ambient conditions. The reasons for improved stability and device performance can be related to 2D perovskite strain relaxation, thermodynamic stability, better crystallinity and barrier separation to oxygen and moisture.

Due to Sb's smaller effective ionic radius when compared to Pb and Sn, there are suitable optoelectronic properties that develop it to become a suitable active layer. Bromoantimonates containing Sb in both valence states (III and V) produced a PCE of nearly 4%. The standard configuration of PSCs shows better performance than the inverted structure. This was confirmed by the findings from Baranwal and coworkers [40]. They used a PSC device architecture of $\text{TiO}_2/(\text{CH}_3\text{NH}_3)_3\text{Sb}_2\text{I}_9/\text{spiro-OMeTAD}$ and $\text{NiO}/(\text{CH}_3\text{NH}_3)_3\text{Sb}_2\text{I}_9/\text{PCBM}$. It was found that the device efficiency was more significant in the case of the former. Sb-based halide perovskites have enhanced stability, especially in ambient and thermal conditions. However, the fabricated devices lack efficiency, which can be related to poor film quality, poor surface morphology and aggravated pinhole formation.

In order to reduce the bandgap of Sb-based perovskites, research is being carried out on practical doping strategies or material engineering (A-site cation replacement). Pal and coworkers showed that introducing Sn^{2+} into $\text{MA}_3\text{Sb}_2\text{I}_9$ can reduce the bandgap by 0.45 eV [41]. However, this was not received well because the decrease in bandgap introduced greater surface roughness. Thus, using an optimal Sn^{2+} content, the resultant device had a balance between surface roughness and bandgap value. Eventually, the resulting device produced a PCE greater than 2.65%. Additionally, doping $\text{MA}_3\text{Sb}_2\text{I}_9$ with Sulfur was also used as a potential light absorber [42]. The resulting device using Sulfur as a dopant produced an efficiency greater than 3.0%.

5.4 $(\text{NH}_4)_3\text{Sb}_2\text{I}_9$ Perovskites

A perovskite-based molecular formula $(\text{NH}_4)_3\text{Sb}_2\text{I}_x\text{Br}_{9-x}$ was synthesised [43]. It was found that, on varying the value of x between 0 and 9, the material was tuned in terms of absorption edges, mobility values and consequently V_{oc} values.

Zuo and coworkers optimised NH_4 -based Sb-halide perovskites by synthesising a series of perovskite materials with varying compositions [44]. This work found that the optical bandgap values varied from 2.27 eV to 2.78 eV. Moreover, on using these varied materials for fabricating a device, the highest record efficiency was 0.51%. Although the efficiency values might be poor, the obtained V_{oc} values were significant, with the highest value being 1003 mV. Figure 4 is a schematic representation of a device using $(\text{NH}_4)_3(\text{Sb}_{(1-x)}\text{Bi}_x)_2\text{I}_9$ as the perovskite material for a switchable photovoltaic study [45,46].

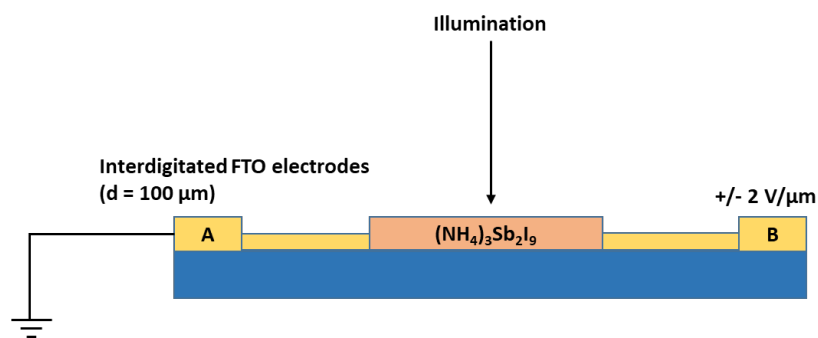


Figure 4. Device configuration with light absorber as $(\text{NH}_4)_3(\text{Sb}_{(1-x)}\text{Bi}_x)_2\text{I}_9$

5.5 Other Sb-based Perovskites

Sb halide-based double perovskites are a domain under constant development as they have been considered the following best material to replace Pb-based PSCs. Karmakar and coworkers showed that Cu^{2+} doping could reportedly improve $\text{Cs}_2\text{SbAgCl}_6$ perovskite performance [11]. The resulting feature showed a reduced indirect bandgap from 2.6 eV to 1.0 eV. Moreover, the device displayed intense structural, photophysical, thermal and moisture stability for more than a year. Using electronic dimensionality principles, by inserting $[\text{M}^{\text{II}}\text{X}_6]$ layers to $\text{Cs}_3\text{Sb}_2\text{X}_9$, double perovskites can be synthesised with lower bandgaps and carrier effective masses. Recently, $\text{FA}_4\text{GeSbCl}_{12}$ double perovskite was produced with a direct bandgap of 1.3 eV [47]. The resulting layer produced a stable and efficient device with a PCE greater than 4.5%.

Adonin and coworkers studied the implementation of N-ethylpyridinium bromoantimonate (N-EtPy) $[\text{SbBr}_6]$ in PSCs [48]. The material was implemented in an inverted PSC, with a bandgap of 2.25 eV (N-EtPy) $[\text{SbBr}_6]$ is a potential candidate for tandem solar cells. (N-EtPy) $[\text{SbBr}_6]$ was used in PSCs with different ETMs (TiO_2 and PCBM). The TiO_2 corresponds to the standard regular device architecture, whereas PCBM corresponds to the inverted architecture. The results showed that the standard device yielded a higher efficiency of 3.8% due to better charge extraction and transportation properties.

Li and coworkers synthesised various 0D Sb-containing perovskite-like materials. The research objective was to identify potential compounds with lower bandgap values to fabricate a high-efficiency PSC [49]. This work identified two heteromorphic hybrid Sb compounds with bandgap values suitable for photovoltaic applications. Jia and coworkers synthesised Cu_3SbI_6 with an indirect bandgap of 2.43 eV [50]. The fabricated device produced a PCE of 0.50% and a V_{oc} value of 704 mV. Vargas and coworkers synthesised a Cu-Sb-based halide perovskite with a direct bandgap of 1.02 eV [51]. $\text{Cs}_4\text{CuSb}_2\text{Cl}_{12}$ displayed excellent stability characteristics, favourable optoelectronic properties and a narrow bandgap.

Nie and coworkers reported a similar structure but with an S-Sb mix to produce MASbSI_2 [52]. The device fabricated using this perovskite-like compound produced a device efficiency of 3.08%. Moreover, the unencapsulated devices showed excellent stability properties where 90% of its initial PCE was retained after dark condition storage. Table 3 summarises the notable Sb-based PSCs that have produced reasonable efficiency values over recent years. In the table 3, PEPDTBT is poly[2,1,3-benzothiadiazole-4,7-diyl[4,4-bis(2-ethylhexyl)-4H-cyclopenta[2,1-b:3,4-b']dithiophene-2,6-diyl]].

Table 3. Photovoltaic performance of notable Antimony Halide PSCs

Device structure	PCE (%)	J_{sc} (mA/cm^2)	V_{oc} (V)	Ref.
ITO/PEDOT:PSS/ $\text{Cs}_3\text{Sb}_2\text{I}_9$ /PCBM/C60/BCP/Al	0.84	2.91	0.60	[24]
FTO/ TiO_2 / $\text{Cs}_3\text{Sb}_2\text{I}_9$ /Au	1.21	3.55	0.61	[29]
FTO/ TiO_2 /m- TiO_2 / $\text{Rb}_3\text{Sb}_2\text{I}_9$ /spiro-OMeTAD/Au	1.37	4.25	0.55	[32]
ITO/PEDOT:PSS/ $\text{Cs}_3\text{Sb}_2\text{I}_9$ /PCBM/Al	1.50	5.31	0.72	[27]
ITO/PEDOT:PSS/ $\text{MA}_3\text{Sb}_2\text{I}_9$ /PCBM/C60/BCP/Al	2.04	5.41	0.62	[24]
FTO/ TiO_2 /m- TiO_2 / $\text{MA}_3\text{Sb}_2\text{I}_{9-x}\text{Cl}_x$ /spiro-OMeTAD/Au	2.19	5.04	0.69	[28]
ITO/Cu:NiO/ $\text{MA}_3(\text{Sb}_{1-x}\text{Sn}_x)_2\text{I}_9$ /ZnO/Al	2.70	8.32	0.56	[39]

FTO/PEDOT:PSS/Pyrene/MA ₃ Sb ₂ I ₉ /PCBM/C60/Al	2.77	6.64	0.7	[38]
FTO/TiO ₂ /m-TiO ₂ /MASbSI ₂ /PEPDTBT/Au	3.08	8.12	0.65	[52]
FTO/TiO ₂ /MA ₃ Sb ₂ I _{9-x} Cl _x /spiro-OMeTAD/Au	3.34	7.38	0.70	[41]
FTO/TiO ₂ /FA ₄ GeSbCl ₁₂ /spiro-OMeTAD/Au	4.70	23.1	0.65	[47]

6. CHALLENGES AND IMPROVEMENT OF ANTIMONY-BASED PEROVSKITES

6.1 Instability due to moisture, temperature and exposure

Sb-based PSCs have shown to produce considerably high PSCs. However, these devices are far from being commercially viable. This is because of the stability values that they are yet to attain. Factors like heat, illumination, air, moisture and oxygen are some parameters we will address in this section.

The exposure of perovskite to severe illumination accelerates its degradation to form products like HI. Pressure, temperature, UV light, and crystallinity have impacted PSC stability. Out of which, moisture-developed degradation is considered to be highly detrimental. Bryant and coworkers showed that illumination-based degradation produces active oxygen, which is the primary reason for the poor operation stability of PSCs. Akbulatov et al. showed how thermal stability of perovskites varies with tuning in A, B and X sites as each perovskite molecule has different light, moisture and O₂ soaking capabilities, which directly impacts PSC stability [53].

Moisture and water content in the atmosphere are essential in determining perovskite surface morphology and device efficiency. The hygroscopic nature of a perovskite molecule degrades the perovskite into the corresponding metal halides and leaves by-products of dihydrates and monohydrates. In some cases, this reaction with water is reversible. Recently, Xu and coworkers showed a numerical simulation explaining the kinetic degradation of perovskite. The study depicted how moisture degradation is majorly started by the structural imperfections of the perovskite molecule [54,55].

Temperature is vital in determining the perovskite structure and phase transition properties. Weber et al. studied how different perovskites gradually degrade with increased temperatures and the variation in crystal geometry [56]. Wang et al. simulated thermal-induced degradation using molecular dynamics [57]. The results showed that the deterioration in the octahedral structure of the perovskite is the primary reason for instability. Additionally, perovskites have low thermal conductivity, causing excessive heat accumulation, and further promoting perovskite degradation.

6.2 Instability due to charge transporting layers

Studies have shown that TiO₂, the commonly used ETM has poor UV light stability. Ito and coworkers further proved that degradation of the perovskite layer could be due to the photocatalytic properties of TiO₂ [58]. Leijtens et al. showed that replacing TiO₂ with Al₂O₃ improved stability as the number of superoxide ions was reduced [59]. Furthermore, studies have shown that PCBM as an ETM leads to degradation under oxygen and moisture. PCBM tends to absorb some degradation products from the perovskite, which collects at the ETM and corrodes the metal electrode.

Sanchez et al. proved that light-induced oxidation of Spiro-OMeTAD leads to interfacial damage [58]. This shows how the operational power of PSCs can be limited because of the degradation at the perovskite/HTM interface. Sekimoto et al. depicted the dependence of perovskite stability through the influence of HTM under light-induced decomposition [59]. The perovskite/HTM was studied significantly, and the electrochemical reaction to form iodine molecules degrades the perovskite. The usage of fullerenes and derived products are known to absorb the degraded products leading to rapid degradation of the perovskite layer.

6.3 Instability due to electrodes

Guerrero et al. characterised various metal electrodes based on their impact on perovskite decomposition through energy profile modification [60]. The degradation of perovskite has been found to degrade due to mobile halide ions, coarse interfacial grains and poor contact. Domanski et al. showed how testing a PSC under MPP conditions displays the slightest deterioration. In contrast, the degradation is rapid and severe in short and open circuit conditions [61].

6.4 Approaches to improve stability

Perovskite material modifications are an effective strategy to yield enhanced PSCs. Studies have shown that partial replacement or introduction of Br with I improves moisture stability. Br has been shown to improve hydrogen bonding with the perovskite molecule, consequently improving device performance and stability. Furthermore, Br is known to reduce the trap state densities of the perovskite film [62]. Xie and coworkers showed that doping is a valuable strategy to increase the device's operational stability and long-term operation [63]. Cao et al. developed a two-step deposition method using Cs and benzylammonium cation, which retained more than 95% of its initial PCE after two months of exposure [64].

Ahmad and coworkers incorporated layered perovskites (2D perovskites) into 3D perovskites to produce devices with enhanced stability [65]. The fabricated devices retained 95% of their initial efficiency despite being unencapsulated and exposed to elevated temperatures and stress for 3000 h. Liang et al. developed a quantum-well thin film using a molten spacer of n-butylamine acetate [66]. The resultant film had uniform grain sizes and enhanced stability under 1100 h of continuous illumination. The crystallinity and surface coverage of the perovskite film is known to impact stability directly. The perovskite stability is known to depend on preparation methods. The resulting film morphology determines the O₂, moisture and grain boundaries influence. Using techniques like solvent engineering is known to improve film quality and stability under dark conditions at humid and elevated temperatures [67].

Additives in the precursor solution are regarded to tremendously improve film stability and efficiency. The addition of polyvinyl alcohol (PVA) increases perovskite film quality and retains 90% of its initial PCE after 30 days of exposure [68]. Jin et al. studied the effect of ZnCl₂ as an additive on PSCs [69]. The partial substitution using ZnCl₂ produces a device with 93% efficiency retention capability compared to the reference devices. Using an optimum concentration of 2 mol% of guanidine sulfamate produces a device with 90.7% PCE retention after 800 h without encapsulation [70].

Along with film modifications, strategies such as modifying the charge transport layers (CTLs), interface engineering and electrode modification contribute to stability development. A well-known fact is that replacing a planar architecture with the corresponding mesoporous structure improves stability considerably [71]. Interface layers across the various films are crucial in improving overall device stability, reducing the initial rapid decay and the slower progressive decay. Defect passivation is another effective strategy to obtain improved PSCs. Dou et al. showed how reproducible, stable, and efficient PSCs can be fabricated using interfacial engineering with CoO [72]. This technique reduces the trap states and dark recombination and improves moisture resistance.

Modifying CTLs through two mechanisms, such as a) improving CTL stability and b) reducing the diffusion of extrinsic factors into the perovskite film, is known to better the PSC stability. The HTM and ETM both impact device stability invariably. Replacing the commonly used HTM, Spiro-OMeTAD and PCBM with hydrophobic polymers demonstrates enhanced PSC stability [73]. Modifying the device by changing the conventionally used electrodes can show higher device stability. Using Cu electrodes shows higher device stability in ambient conditions rather than the Al-based electrodes [74]. The fabricated device could perform efficiently without any PCE losses after 20 days.

Table 4. Stability of Antimony-based PSCs

Material	PCE (%)	Stability properties	Ref.
Cs ₃ Sb ₂ I ₉	< 1.0	More stable in ambient conditions than MAPbI ₃	[6]
MA ₂ AgSbI ₆	-	Stable at room temperature for 370 days (20-60% humidity)	[20]
MASbSI ₂	3.08	90% of initial PCE is retained after 15 days of dark storage (60% humidity and 25 °C)	[50]
(NH ₄) ₃ Sb ₂ I ₉	0.51	80% of initial PCE is retained in a glovebox for 40 days (O ₂ < 10 ppm, H ₂ O < 0.1 ppm). Lost performance entirely at 50% humidity	[17]

The final component of a PSC is encapsulation. This plays a vital role in determining the overall device stability and lifetime. Studies have proved that a device performs better without encapsulation in low-humid environments.

However, an encapsulated device can perform exceptionally well in operational conditions through various temperatures and moisture levels. It hinders the degradation of the subsequent layers in the device by behaving as a protective film. Recent research showed that devices can have increased moisture and temperature resistance by having a thin layer of ALD amorphous oxide ETM. Fu et al. showed that using Si-based photovoltaics encapsulant is unsuitable for perovskites because of high laminated temperatures [75]. Encapsulation using PU is done at a slightly lower temperature. It is known to improve the thermal stability of the device. However, encapsulation is also known to do more harm than good regarding stability tests and device performance. The encapsulation process involves intense thermal stress, UV curing, pressure and sealing mechanisms that only lead to PCE loss but harms the film quality [76].

Hysteresis is a common phenomenon observed in nearly all fabricated PSCs. There is no definite reason as to why hysteresis occurs. However, their origins are charge carriers trapping/de-trapping, ferroelectric polarisation, capacitive effects, charge accumulation and ion migration. The hysteresis effect is more prominent in planar PSCs but is equally visible in mesoporous-based devices [77].

Shao et al. approached this problem using fullerene layer deposition on perovskites to reduce charge trapping and, thus, remove hysteresis [78]. Zhong et al. also studied the impact of using PCBM as a passivator to remove device hysteresis [79]. A commonly used method to eliminate/minimise hysteresis in mesoporous and planar structures is doping the perovskite with potassium iodide [80]. This can be related to the reduced ion migration and stable perovskite/CTL interface.

Techniques like surface passivation, partial substitution, additives and deoxidisers have been used to address the stability concerns of Sb-based perovskites. Surface passivation is a technique where defects or recombination sites on the surface of the perovskite film are eradicated through a molecular-binding technique [81]. This method dramatically reduces charge recombination and promotes charge transfer to a greater extent. Using this method, the improvement in device efficiency will be gradual, steady, but notable as there is a considerable change in the crystal structure. Surface passivation is known to stabilise perovskite nanocrystals effectively.

Partial substitution involves tuning the perovskite molecule with atoms/compounds that can modulate the perovskite material properties [82]. This modulation can happen in terms of stability, film formation and efficiency. These improved properties can be observed notably by partially substituting either the A, B or X ions, as they significantly contribute to device performance.

Additives and deoxidisers are often used to facilitate better stability properties. Additives can be organic or inorganic chemicals added in a regulated amount to the perovskite solution. Some of the notable examples include: Ammonium Chloride (NH_4Cl) and 2,2,2-trifluoroethylamine hydrochloride (TFEACI) [83,84]. Reducing agents or deoxidisers are commonly used to restrict the oxidation process of metal ions [85]. Examples include Ascorbic acid, Hydrazine and Hydrophosphorous acid. Moreover, in ideal cases, deoxidisers play a dual role wherein they behave as oxygen scavengers and as phase separation inhibitor [86].

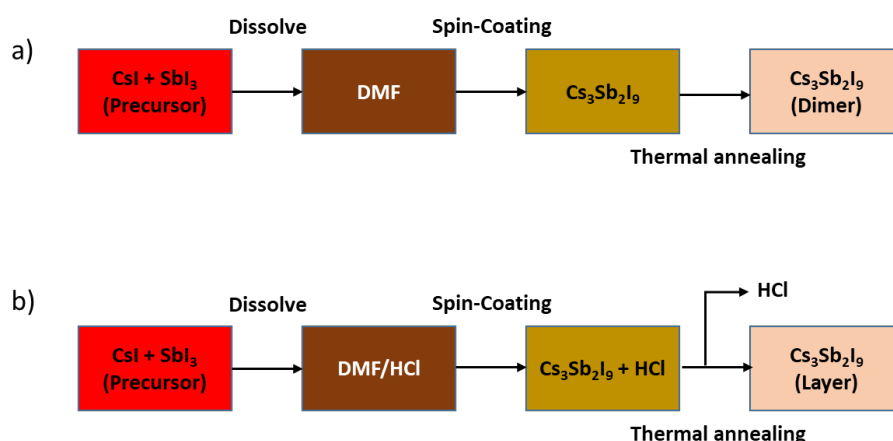


Figure 5. Flowchart representing an antisolvent preparatory method for the layered and dimeric form of $\text{Cs}_3\text{Sb}_2\text{I}_9$

7. CONCLUSION

This review identifies the need for computational and experimental calculations, especially in Sb-based perovskite solar cells. Moreover, we also examined the various works and strategies researchers have used to improve device performance. The concept was further expanded to double perovskites as well.

It is necessary to highlight that, be it for any perovskite film, the device performance is dependent on the perovskite structure, vacancy states, optoelectronic material properties, binding energy, diffusion lengths and structural properties. In most cases, finding favourable material in all these categories is not easy. Thus, techniques like doping, material engineering, compositional engineering and lattice dimension modifications must be implemented to develop a robust Sb-based perovskite for improved photovoltaic performance [87]. However, the work is not just limited to material characteristics but can be expanded to the deposition and preparation methods. Novel methods are constantly increasing to modulate and regulate the perovskite crystal size.

In this review, we can conclude the pressing need to use computational and theoretical studies coupled with experimental studies to verify specific findings. These findings are the instability associated with the material or device, the need for doping and engineering modifications, long-term stability and barriers to commercialisation. Dubey and coworkers have suggested that the path for perovskite solar cells is immense mainly due to the amount of research pending in solvent and precursor selection, film thickness, temperature, growth condition and additive studies [88]. Moreover, Zhang and Gao's works suggested that incorporating low bandgap polymers above the perovskite layer is a viable strategy to improve photovoltaic performance [89,90].

Currently, most of the research on PSCs focuses on improving performance, studying device materials, optical and electrical properties, charge carriers and dynamics. There are several studies on various deposition techniques, organic-inorganic material frameworks, interfacial and molecular engineering, and technologies to develop commercially viable large-scale solar modules. However, LCA results have shown that we must address the toxicity of Pb-based PSCs and bring these devices in line with commercially competitive standards. Strategies such as material engineering, interfacial engineering, encapsulation methods and choice of device materials have been adopted to address device stability. A major issue that one can observe is the scalability of this technology. The reproducibility and upgradation from a lab to the industry are still unclear. Lastly, the production of PSCs should be analysed regarding scalability and toxicity, especially when comparing other photovoltaic technologies [91].

The significant challenges of Sb-based perovskite materials are a) wide bandgaps, b) poor morphology, c) incompatible charge transport materials, and d) water sensitivity. Thus, research needs to continue inserting less-toxic metals suitable antisolvents and develop new additives, improve interfacial contact between the perovskite and charge transport materials, synthesise hydrophobic interlayers, or incorporate cations into the perovskite structure [92].

VA-based perovskites are also subject to large bandgaps, phase separation, grain boundaries, interfacial recombination, high defect states and poor performance. Antimony is a one-of-a-kind material which varies between 0D to 3D structures, giving it an enhanced structural dimension and unique optoelectronic properties [92,93]. Thus, up-and-coming research should focus on how these materials can break the abovementioned barriers to produce eco-friendly devices. Research can also be conducted on how various Sb-synthesised perovskite films perform with a variation in halide and A-site ions, forming an integral part of the device. Lastly, looking into the interface and quality of films is of utmost importance. One needs to keep a tab on the film quality produced and how various fabrication strategies can play a vital role in determining favourable device performance [94,95].

REFERENCES

- [1] Thomas, A. (2022). High-Efficiency Dye-Sensitized Solar Cells: A Comprehensive Review. *Computational And Experimental Research In Materials And Renewable Energy*, 5(1), 1. doi: 10.19184/cerimre.v5i1.31475
- [2] Hayat, Muhammad & Ali, Danish & Monyake, Cathrine & Alagha, Lana & Ahmed, Niaz. (2018). Solar energy—A look into power generation, challenges, and a solar-powered future. *International Journal of Energy Research*. 43. 10.1002/er.4252.
- [3] Jin, Z., Zhang, Z., Xiu, J., Song, H., Gatti, T., & He, Z. (2020). A critical review on bismuth and antimony halide based perovskites and their derivatives for photovoltaic applications: recent advances and challenges. *Journal Of Materials Chemistry A*, 8(32), 16166-16188. doi: 10.1039/d0ta05433j.
- [4] Leccisi E and Fthenakis V, Life-cycle environmental impacts of singlejunction and tandem perovskite PVs:

- a critical review and future perspectives. *Prog Energy* 2:032002 (2020).
- [5] Schileo G and Grancini G, Lead or no lead? Availability, toxicity, sustainability and environmental impact of lead-free perovskite solar cells. *J Mater Chem C* 9:67–76 (2021).
- [6] Thornton, S.T., Abdelmageed, G., Kahwagi, R.F. and Koleilat, G.I. (2022), progress towards lead-free, efficient, and stable perovskite solar cells. *J Chem Technol Biotechnol*, 97: 810-829. <https://doi.org/10.1002/jctb.6830>
- [7] Liao W, Zhao D, Yu Y, Grice CR, Wang C, Cimaroli AJ et al., Lead-free inverted planar formamidinium tin triiodide perovskite solar cells achieving power conversion efficiencies up to 6.22%. *Adv Mater* 28:9333–9340 (2016).
- [8] B. Saparov, F. Hong, J.-P. Sun, H.-S. Duan, W. Meng, S. Cameron, I. G. Hill, Y. Yan and D. B. Mitzi, *Chem. Mater.*, 2015, 27, 5622-5632.
- [9] J.-P. Correa-Baena, L. Nienhaus, R. C. Kurchin, S. S. Shin, S. Wiegold, N. T. Putri Hartono, M. Layurova, N. D. Klein, J. R. Poindexter, A. Polizzotti, S. Sun, M. G. Bawendi and T. Buonassisi, *Chem. Mater.*, 2018, 30, 3734-3742.
- [10] J. Pal, S. Manna, A. Mondal, S. Das, K. V. Adarsh and A. Nag, *Angew. Chem. Int. Edit.*, 2017, 56, 14187-14191.
- [11] A. Karmakar, M. S. Dodd, S. Agnihotri, E. Ravera and V. K. Michaelis, *Chem. Mater.*, 2018, 30, 8280-8290.
- [12] G. Tang, Z. Xiao, H. Hosono, T. Kamiya, D. Fang and J. Hong, *J. Phys. Chem. Lett.*, 2018, 9, 43-48.
- [13] B. Vargas, R. Torres-Cadena, J. Rodríguez-Hernández, M. Gembicky, H. Xie, J. Jiménez-Mier, Y.-S. Liu, E. Menéndez-Proupin, K. R. Dunbar, N. Lopez, P. Olalde-Velasco and D. Solis-Ibarra, *Chem. Mater.*, 2018, 30, 5315-5321.
- [14] Jakubas, R.; Decressain, R.; Lefebvre, J. NMR and Dilatometric Studies of the Structure Phase transitions of (CH₃NH₃)₃Sb₂I₉, and (CH₃NH₃)₃Bi₂I₉ Crystal. *J. Phys. Chem. Solids* 1992, 53, 755–759.
- [15] Bagautdinov, B.; Novikova, M. S.; Aleksandrova, I. P.; Blomberg, M. K.; Chapuis, G. X-ray study of phase transitions in Cs₃Sb₂I₉ crystal. *Solid State Commun.* 1999, 111, 361–366.
- [16] Yang, Y.; Liu, C.; Cai, M.; Liao, Y.; Ding, Y.; Ma, S.; Liu, X.; Guli, M.; Dai, S.; Nazeeruddin, M. K. Dimension-controlled Growth of Antimony-based Perovskite-like Halide for Lead-free and Semitransparent Photovoltaics. *ACS Appl. Mater. Interfaces* 2020, 12, 17062–17069.
- [17] Zhang, H.; Fang, L.; Yuan, R.-Z. Triammonium nonaiododiantimonate(III), (NH₄)₃[Sb₂I₉]. *Acta Crystallogr., Sect. E: Struct. Rep. Online* 2005, 61, i70–i72.
- [18] Zuo, C.; Ding, L. Lead-free Perovskite Materials (NH₄)₃Sb₂I_xBr_{9-x}. *Angew. Chem., Int. Ed.* 2017, 56, 6528–6532.
- [19] X.-G. Zhao, J.-H. Yang, Y. Fu, D. Yang, Q. Xu, L. Yu, S.-H. Wei and L. Zhang, *J. Am. Chem. Soc.*, 2017, 139, 2630-2638.
- [20] C. Zuo, L. Ding, *Angew. Chem.* 2017, 129, 6628.
- [21] R. X. Yang, K. T. Butler and A. Walsh, *J. Phys. Chem. Lett.*, 2015, 6, 5009-5014.
- [22] Li, Y.-J.; Wu, T.; Sun, L.; Yang; et al. Lead-free and Stable Antimony–Silver-Halide Double Perovskite (CH₃NH₃)₂AgSbI₆. *RSC Adv.* 2017, 7, 35175–35180
- [23] Zuo, C.; Ding, L. Lead-free Perovskite Materials (NH₄)₃Sb₂I_xBr_{9-x}. *Angew. Chem., Int. Ed.* 2017, 56, 6528–6532.
- [24] Boopathi, K. M.; Karuppuswamy, P.; Singh, A.; Hanmandlu, C.; Lin, L.; Abbas, S. A.; Chang, C. C.; Wang, P. C.; Li, G.; Chu, C. W. Solution-Processable Antimony-based Light-absorbing Materials Beyond Lead Halide Perovskites. *J. Mater. Chem. A* 2017, 5, 20843–20850.
- [25] B. Saparov, F. Hong, J.-P. Sun, H.-S. Duan, W. Meng, S. Cameron, I. G. Hill, Y. Yan and D. B. Mitzi, *Chem. Mater.*, 2015, 27, 5622-5632.
- [26] H. C. Sansom, G. F. S. Whitehead, M. S. Dyer, M. Zanella, T. D. Manning, M. J. Pitcher, T. J. Whittles, V. R. Dhanak, J. Alaria, J. B. Claridge and M. J. Rosseinsky, *Chem. Mater.*, 2017, 29, 1538–1549. J.-P. Correa-Baena, L. Nienhaus, R. C. Kurchin, S. S. Shin, S. Wiegold, N. T. Putri Hartono, M. Layurova, N. D. Klein, J. R. Poindexter, A. Polizzotti, S. Sun, M. G. Bawendi and T. Buonassisi, *Chem. Mater.*, 2018, 30, 3734-3742.
- [27] A. Singh, K. M. Boopathi, A. Mohapatra, Y. F. Chen, G. Li and C. W. Chu, *ACS Appl. Mater. Interfaces*, 2018, 10, 2566-2573.
- [28] F. Jiang, D. Yang, Y. Jiang, T. Liu, X. Zhao, Y. Ming, B. Luo, F. Qin, J. Fan, H. Han, L. Zhang and Y. Zhou,

- J. Am. Chem. Soc., 2018, 140, 1019-1027.
- [29] F. Umar, J. Zhang, Z. Jin, I. Muhammad, X. Yang, H. Deng, K. Jahangeer, Q. Hu, H. Song and J. Tang, *Adv. Opt. Mater.*, 2019, 7, 1801368.
- [30] Chonamada, T. D.; Dey, A. B.; Santra, P. K. Degradation Studies of Cs₃Sb₂I₉: A Lead-Free Perovskite. *ACS Appl. Energy Mater.* 2020, 3, 47–55.
- [31] Harikesh, P. C.; Mulmudi, H. K.; Ghosh, B.; Goh, T. W.; Teng, Y. T.; Thirumal, K.; Lockrey, M.; Weber, K.; Koh, T. M.; Li, S.; Mhaisalkar, S.; Mathews, N. Rb as an Alternative Cation for Templating Inorganic Lead-Free Perovskites for Solution Processed Photovoltaics. *Chem. Mater.* 2016, 28, 7496–7504.
- [32] S. Weber, T. Rath, K. Fellner, R. Fischer, R. Resel, B. Kunert, T. Dimopoulos, A. Steinegger and G. Trimmel, *ACS Appl. Energy Mater.*, 2019, 2, 539-547.
- [33] Li, F.; Wang, Y.; Xia, K.; Hoye, R. L. Z.; Pecunia, V. Microstructural and Photoconversion Efficiency Enhancement of Compact Films of Lead-Free Perovskite Derivative Rb₃Sb₂I₉. *J. Mater. Chem. A* 2020, 8, 4396–4406.
- [34] Hebig, J. C.; Kühn, I.; Flohre, J.; Kirchartz, T. Optoelectronic Properties of (CH₃NH₃)₃Sb₂I₉ Thin Films for Photovoltaic Applications. *ACS Energy Lett.* 2016, 1, 309–314.
- [35] Recent Progress and Challenges in A₃Sb₂X₉-Based Perovskite Solar Cells Khursheed Ahmad and Shaikh M. Mobin *ACS Omega* 2020 5 (44), 28404-28412 DOI: 10.1021/acsomega.0c04174
- [36] Ahmad, K.; Kumar, P.; Mobin, S. M. A Two-Step Modified Sequential Deposition Method-based Pb-Free (CH₃NH₃)₃Sb₂I₉ Perovskite with Improved Open Circuit Voltage and Performance. *ChemElectroChem* 2020, 7, 946–950.
- [37] Giesbrecht, N.; Weis, A.; Bein, T. Formation of stable 2D Methylammonium Antimony Iodide Phase for Lead-free Perovskitelike Solar Cells. *J. Phys.: Energy* 2020, 2, 024007.
- [38] Karuppuswamy P, Boopathi KM, Mohapatra A, Chen H-C, Wong K-T, Wang P-C et al., Role of a hydrophobic scaffold in controlling the crystallisation of methylammonium antimony iodide for efficient lead-free perovskite solar cells. *Nano Energy* 45:330–336 (2018).
- [39] Y. Yang, C. Liu, M. Cai, Y. Liao, Y. Ding, S. Ma, X. Liu, M. Guli, S. Dai and M. K. Nazeeruddin, *ACS Appl. Mater. Interfaces*, 2020, 12, 17062-17069.
- [40] A. K. Baranwal, H. Masutani, H. Sugita, H. Kanda, S. Kanaya, N. Shibayama, Y. Sanehira, M. Ikegami, Y. Numata, K. Yamada, T. Miyasaka, T. Umeyama, H. Imahori, S. Ito, *Nano Convergence* 2017, 4, 26.
- [41] Chatterjee, S.; Pal, A. J. Tin(IV) Substitution in (CH₃NH₃)₃Sb₂I₉: Towards Low Band Gap Defect-Ordered Hybrid Perovskite Solar Cells. *ACS Appl. Mater. Interfaces* 2018, 10, 35194–35205.
- [42] Chatterjee, S.; Pal, A. J. Tin(IV) Substitution in (CH₃NH₃)₃Sb₂I₉: Towards Low Band Gap Defect-Ordered Hybrid Perovskite Solar Cells. *ACS Appl. Mater. Interfaces* 2018, 10, 35194–35205.
- [43] T. Li, X. Wang, Y. Yan and D. B. Mitzi, *J. Phys. Chem. Lett.*, 2018, 9, 3829-3833
- [44] C. Zuo and L. Ding, *Angew. Chem. Int. Edit.*, 2017, 56, 6528-6532
- [45] Sani F, Shafie S, Lim HN, Musa AO. Advancement on Lead-Free Organic-Inorganic Halide Perovskite Solar Cells: A Review. *Materials (Basel)*. 2018 Jun 14;11(6):1008. doi: 10.3390/ma11061008. PMID: 29899206; PMCID: PMC6024904.
- [46] Jin, Z., Zhang, Z., Xiu, J., Song, H., Gatti, T., & He, Z. (2020). A critical review on bismuth and antimony halide based perovskites and their derivatives for photovoltaic applications: recent advances and challenges. *Journal Of Materials Chemistry A*, 8(32), 16166-16188. doi: 10.1039/d0ta05433j
- [47] W. B. Dai, S. Xu, J. Zhou, J. Hu, K. Huang and M. Xu, *Sol. Energy Mater. Sol. C.*, 2019, 192, 140-146.
- [48] Adonin, S. A.; Frolova, L. A.; Sokolov, M. N.; Shilov, G. V.; Korchagin.; et al. Antimony (V) Complex Halides: Lead-Perovskite-Like Materials for Hybrid Solar Cells. *Adv. Energy Mater.* 2018, 8, 1701140.
- [49] Li, Y.; Xu, Z.; Liu, X.; Tao.; et al. Two Heteromorphic Crystals of Antimony-Based Hybrids Showing Tunable Optical Band Gaps and Distinct Photoelectric Responses. *Inorg. Chem.* 2019, 58, 6544–6549
- [50] Jia, X.; Ding, L. A Low-temperature Solution-processed Copper Antimony Iodide Rudorffite for Solar Cells. *Sci. China Mater.* 2019, 62, 54–58.
- [51] Vargas, B.; Ramos, E.; Perez- Gutierrez, E.; Alonso, J. C.; Solis-Ibarra, D. A Direct Bandgap Copper–Antimony Halide Perovskite. *J. Am. Chem. Soc.* 2017, 139, 9116–9119.
- [52] Nie, R.; Mehta, A.; Park, B.-W.; Kwon, H.-W.; Im, J.; Seok, S. I. Mixed sulfur and iodide-based lead-free perovskite solar cells. *J. Am. Chem. Soc.* 2018, 140, 872–875.
- [53] A.F. Akbulatov, L.A. Frolova, N.N. Dremova, I. Zhidkov, V.M. Martynenko, S. A. Tsarev, S.Y. Luchkin,

- E.Z. Kurmaev, S.M. Aldoshin, K.J. Stevenson, P. A. Troshin, Light or heat: what is killing lead halide perovskites under solar cell operation conditions? *J. Phys. Chem. Lett.* 11 (2020) 333–339, <https://doi.org/10.1021/acs.jpcclett.9b03308>.
- [54] A. Poglitsch, D. Weber, Dynamic disorder in methylammoniumtrihalogenoplumbates (II) observed by millimeter-wave spectroscopy, *J. Chem. Phys.* 87 (1987) 6373–6378, <https://doi.org/10.1063/1.453467>.
- [55] M. Wang, V. Vasudevan, S. Lin, J. Jasieniak, S.P. Russo, N. Birbilis, N. V. Medhekar, Molecular mechanisms of thermal instability in hybrid perovskitelight absorbers for photovoltaic solar cells, *J. Mater. Chem. A* 8 (2020) 17765–17779, <https://doi.org/10.1039/d0ta05356b>.
- [56] S. Ito, S. Tanaka, K. Manabe, H. Nishino, Effects of surface blocking layer of Sb₂S₃ on nanocrystalline TiO₂ for CH₃NH₃PbI₃ perovskite solar cells, *J. Phys. Chem. C* 118 (2014) 16995–17000, <https://doi.org/10.1021/jp500449z>.
- [57] T. Leijtens, G.E. Eperon, S. Pathak, A. Abate, M.M. Lee, H.J. Snaith, Overcoming ultraviolet light instability of sensitized TiO₂ with meso-superstructured organometal tri-halide perovskite solar cells, *Nat. Commun.* 4 (2013) 1–8, <https://doi.org/10.1038/ncomms3885>.
- [58] R.S. Sanchez, E. Mas-Marza, Light-induced effects on Spiro-OMeTAD films and hybrid lead halide perovskite solar cells, *Sol. Energy Mater. Sol. Cells* 158 (2016) 189–194, <https://doi.org/10.1016/j.solmat.2016.03.024>.
- [59] T. Sekimoto, T. Matsui, T. Nishihara, R. Uchida, T. Sekiguchi, T. Negami, Influence of a hole-transport layer on light-induced degradation of mixed organicoorganic halide perovskite solar cells, *ACS Appl. Energy Mater.* 2 (2019) 5039–5049, <https://doi.org/10.1021/acsaem.9b00709>.
- [60] A. Guerrero, J. You, C. Aranda, Y.S. Kang, G. Garcia-Belmonte, H. Zhou, J. Bisquert, Y. Yang, Interfacial degradation of planar lead halide perovskite solar cells, *ACS Nano* 10 (2016) 218–224, <https://doi.org/10.1021/acsnano.5b03687>.
- [61] K. Domanski, E.A. Alharbi, A. Hagfeldt, M. Grätzel, W. Tress, Systematic investigation of the impact of operation conditions on the degradation behaviour of perovskite solar cells, *Nat. Energy* 3 (2018) 61–67, <https://doi.org/10.1038/s41560-017-0060-5>.
- [62] J.H. Noh, S.H. Im, J.H. Heo, T.N. Mandal, S. Il Seok, Chemical management for colorful, efficient, and stable inorganic-organic hybrid nanostructured solar cells, *Nano Lett.* 13 (2013) 1764–1769, <https://doi.org/10.1021/nl400349b>.
- [63] L. Xie, P. Song, L. Shen, J. Lu, K. Liu, K. Lin, W. Feng, C. Tian, Z. Wei, Revealing the compositional effect on the intrinsic long-term stability of perovskite solar cells, *J. Mater. Chem. A* 8 (2020) 7653–7658, <https://doi.org/10.1039/d0ta01668c>.
- [64] J. Cao, J. Jiang, N. Li, Y. Dong, Y. Jia, S. Tao, N. Zhao, Alkali-cation-enhanced benzylammonium passivation for efficient and stable perovskite solar cells fabricated through sequential deposition, *J. Mater. Chem. A* 8 (2020) 19357–19366, <https://doi.org/10.1039/d0ta04680a>.
- [65] S. Ahmad, P. Fu, S. Yu, Q. Yang, X. Liu, X. Wang, X. Wang, X. Guo, C. Li, Dionjacobson phase 2D layered perovskites for solar cells with ultrahigh stability, *Joule* 3 (2019) 794–806, <https://doi.org/10.1016/j.joule.2018.11.026>.
- [66] C. Liang, H. Gu, Y. Xia, Z. Wang, X. Liu, J. Xia, S. Zuo, Y. Hu, X. Gao, W. Hui, L. Chao, T. Niu, M. Fang, H. Lu, H. Dong, H. Yu, S. Chen, X. Ran, L. Song, B. Li, J. Zhang, Y. Peng, G. Shao, J. Wang, Y. Chen, G. Xing, W. Huang, Twodimensional Ruddlesden–Popper layered perovskite solar cells based on phasepure thin films, *Nat. Energy* 6 (2021) 38–45, <https://doi.org/10.1038/s41560-020-00721-5>.
- [67] J.H. Kim, S.T. Williams, N. Cho, C.C. Chueh, A.K.Y. Jen, Enhanced environmental stability of planar heterojunction perovskite solar cells based on blade-coating, *Adv. Energy Mater.* 5 (2015) 2–7, <https://doi.org/10.1002/aenm.201401229>.
- [68] Y. Sun, Y. Wu, X. Fang, L. Xu, Z. Ma, Y. Lu, W.H. Zhang, Q. Yu, N. Yuan, J. Ding, Long-term stability of organic-inorganic hybrid perovskite solar cells with high efficiency under high humidity conditions, *J. Mater. Chem. A* 5 (2017) 1374–1379, <https://doi.org/10.1039/c6ta08117g>.
- [69] J. Jin, H. Li, C. Chen, B. Zhang, L. Xu, B. Dong, H. Song, Q. Dai, Enhanced performance of perovskite solar cells with zinc chloride additives, *ACS Appl. Mater. Interfaces* 9 (2017) 42875–42882, <https://doi.org/10.1021/acsaami.7b15310>.
- [70] X. Liu, J. Wu, Y. Yang, D. Wang, G. Li, X. Wang, W. Sun, Y. Wei, Y. Huang, M. Huang, L. Fan, Z. Lan, J. Lin, K.C. Ho, Additive engineering by bifunctional guanidine sulfamate for highly efficient and stable

- perovskites solar cells, *Small* 16 (2020) 1–9, <https://doi.org/10.1002/sml.202004877>.
- [71] S. Castro-Hermosa, S.K. Yadav, L. Vesce, A. Guidobaldi, A. Reale, A. Di Carlo, T. M. Brown, Stability issues pertaining large area perovskite and dye-sensitized solar cells and modules, *J. Phys. D Appl. Phys.* 50 (2017), 33001, <https://doi.org/10.1088/1361-6463/50/3/033001>.
- [72] Y. Dou, D. Wang, G. Li, Y. Liao, W. Sun, J. Wu, Z. Lan, Toward highly reproducible, efficient, and stable perovskite solar cells via interface engineering with CoO nanoplates, *ACS Appl. Mater. Interfaces* 11 (2019) 32159–32168, <https://doi.org/10.1021/acsami.9b11039>.
- [73] F. Hou, F. Jin, B. Chu, Z. Su, Y. Gao, H. Zhao, P. Cheng, J. Tang, W. Li, Hydrophobic hole-transporting layer induced porous PbI₂ film for stable and efficient perovskite solar cells in 50% humidity, *Sol. Energy Mater. Sol. Cells* 157 (2016) 989–995, <https://doi.org/10.1016/j.solmat.2016.08.024>.
- [74] Y. Deng, Q. Dong, C. Bi, Y. Yuan, J. Huang, Air-stable, efficient mixed-cation perovskite solar cells with Cu electrode by scalable fabrication of active layer, *Adv. Energy Mater.* 6 (2016) 1–6, <https://doi.org/10.1002/aenm.201600372>.
- [75] Z. Fu, M. Xu, Y. Sheng, Z. Yan, J. Meng, C. Tong, D. Li, Z. Wan, Y. Ming, A. Mei, Y. Hu, Y. Rong, H. Han, Encapsulation of printable mesoscopic perovskite solar cells enables high temperature and long-term outdoor stability, *Adv. Funct. Mater.* 29 (2019) 1–7, <https://doi.org/10.1002/adfm.201809129>.
- [76] F. Matteocci, L. Cin`a, E. Lamanna, S. Cacovich, G. Divitini, P.A. Midgley, C. Ducati, A. Di Carlo, Encapsulation for long-term stability enhancement of perovskite solar cells, *Nano Energy* 30 (2016) 162–172, <https://doi.org/10.1016/j.nanoen.2016.09.041>.
- [77] L. Meng, J. You, T.F. Guo, Y. Yang, Recent advances in the inverted planar structure of perovskite solar cells, *Acc. Chem. Res.* 49 (2016) 155–165, <https://doi.org/10.1021/acs.accounts.5b00404>.
- [78] Y. Shao, Z. Xiao, C. Bi, Y. Yuan, J. Huang, Origin and elimination of photocurrent hysteresis by fullerene passivation in CH₃NH₃PbI₃ planar heterojunction solar cells, *Nat. Commun.* 5 (2014) 1–7, <https://doi.org/10.1038/ncomms6784>.
- [79] Y. Zhong, M. Hufnagel, M. Thelakkat, C. Li, S. Huettner, Role of PCBM in the suppression of hysteresis in perovskite solar cells, *Adv. Funct. Mater.* 30 (2020), <https://doi.org/10.1002/adfm.201908920>.
- [80] D.Y. Son, S.G. Kim, J.Y. Seo, S.H. Lee, H. Shin, D. Lee, N.G. Park, Universal approach toward hysteresis-free perovskite solar cell via defect engineering, *J. Am. Chem. Soc.* 140 (2018) 1358–1364, <https://doi.org/10.1021/jacs.7b10430>.
- [81] Dibyajyoti Saikia, Atanu Betal, Jayanta Bera, Satyajit Sahu, Progress and challenges of halide perovskite-based solar cell- a brief review, *Materials Science in Semiconductor Processing*, Volume 150, 2022, 106953, ISSN 1369-8001, <https://doi.org/10.1016/j.mssp.2022.106953>.
- [82] Bonabi Naghadeh S, Luo B, Abdelmageed G, Pu Y-C, Zhang C and Zhang JZ, Photophysical properties and improved stability of organic–inorganic perovskite by surface passivation. *J Phys Chem C* 122:15799–15818 (2018).
- [83] Kopacic I, Friesenbichler B, Hoefler SF, Kunert B, Plank H, Rath T et al., Enhanced performance of germanium halide perovskite solar cells through compositional engineering. *ACS Appl Energy Mater* 1: 343–347 (2018).
- [84] Xu H, Jiang Y, He T, Li S, Wang H, Chen Y et al., Orientation regulation of tin-based reduced-dimensional perovskites for highly efficient and stable Photovoltaics. *Adv Funct Mater* 29:1807696 (2019).
- [85] Yu B-B, Liao M, Yang J, Chen W, Zhu Y, Zhang X et al., Alloy-induced phase transition and enhanced photovoltaic performance: the case of Cs₃Bi₂I₉–xBr_x perovskite solar cells. *J Mater Chem A* 7:8818–8825 (2019).
- [86] Xu X, Chueh C-C, Yang Z, Rajagopal A, Xu J, Jo SB et al., Ascorbic acid as an effective antioxidant additive to enhance the efficiency and stability of Pb/Sn-based binary perovskite solar cells. *Nano Energy* 34:392–398 (2017).
- [87] Tai Q, Guo X, Tang G, You P, Ng T-W, Shen D et al., Antioxidant grain passivation for air-stable tin-based perovskite solar cells. *Angew Chem Int Ed* 58:806–810 (2019).
- [88] Dubey A, Adhikari N, Mabrouk S, Wu F, Chen K, Yang S et al., A strategic review on processing routes towards highly efficient perovskite solar cells. *J Mater Chem A* 6:2406–2431 (2018).
- [89] Zhang, S.; Ye, L.; Zhao, W.; Yang, B.; Wang, Q.; Hou, J. Realising over 10% efficiency in polymer solar cell by device optimisation. *Sci. China Chem.* 2015, 58, 248–256.
- [90] Gao, K.; Zhu, Z.; Xu, B.; Jo, S.; Kan, Y.; Peng, X.; Jen, A.K. Highly Efficient Porphyrin-Based

- OPV/Perovskite Hybrid Solar Cells with Extended Photoresponse and High Fill Factor. *Adv. Mater.* 2017, 29, 1703980.
- [91] Thomas, A. S. Synthesis and Efficiency Analysis of Perovskite Solar Cells.
- [92] Thomas, A.S. Film Properties Using Metal Salts Washing for Perovskite Solar Cells. Preprints 2022, 2022070192 (doi: 10.20944/preprints202207.0192.v1).
- [93] Thomas, Ankit Stephen. 2022. "Charge Transport Materials, Bismuth and Copper-Based Perovskite Solar Cells: A Review". *Future Energy* 1 (3):19-43. <https://fupubco.com/fuen/article/view/30>.
- [94] AWakamiya, M. Endo, T. Sasamori, N. Tokitoh, Y. Ogomi, S. Hayase, Y. Murata, Reproducible fabrication of efficient perovskite-based solar cells: X-ray crystallographic studies on the formation of CH₃NH₃PbI₃ layers, *Chem. Lett.* 43 (2014) 711–713, <https://doi.org/10.1246/cl.140074>.
- [95] A.M.A. Leguy, Y. Hu, M. Campoy-Quiles, M.I. Alonso, O.J. Weber, P. Azarhoosh, M. Van Schilfgaarde, M.T. Weller, T. Bein, J. Nelson, P. Docampo, P.R.F. Barnes, Reversible hydration of CH₃NH₃PbI₃ in films, single crystals, and solar cells *Chem. Mater.* 27 (2015) 3397–3407, <https://doi.org/10.1021/acs.chemmater.5b00660>.